Journal of Alloys and Compounds 508 (2010) 55–61

Contents lists available at ScienceDirect

Journal of Alloys and Compounds

journal homepage: www.elsevier.com/locate/jallcom

Prediction of concomitant structures in binary metallic systems from *RG* map: With $MgCu_2$ structure type as an example

V.L. Kameswari [a], V. Seshubai [a,*], T. Rajasekharan [b]

[a] School of Physics, University of Hyderabad, Gachibowli P.O., Hyderabad, 500 046, India
[b] Defence Metallurgical Research Laboratory, Kanchanbagh P.O., Hyderabad, 500 058, India

ARTICLE INFO

Article history:
Received 1 June 2010
Received in revised form 29 July 2010
Accepted 30 July 2010
Available online 12 August 2010

Keywords:
Intermetallics
Phase diagrams
Concomitant structures
Laves phases
Miedema's parameters
Crystal chemistry

ABSTRACT

The efficacy of Rajasekharan–Girgis (*RG*) maps, constructed using Miedema's parameters, in predicting concomitant structure types in metallic binary systems is discussed taking $MgCu_2$ structure type as an example. 22 structure types that are concomitant with $MgCu_2$ type compounds are studied on the *RG* map and the salient points are discussed. The map can tell us, for instance, that in the Ho–Ni binary system where the $HoNi_2$ compound is of $MgCu_2$ type structure, $HoNi_3$ and $NiHo_3$ are likely to stabilize with $NbBe_3$ and CFe_3 type structures respectively, and not vice versa. The occurrence of $CuAl_2$ type structure, rather than $MgCu_2$ type, in certain binary systems with atomic radii ratio 1.225 considered 'ideal' for the formation of $MgCu_2$ type compounds, is explained. The *RG* map can minimize the set of candidate structures on which quantum mechanical calculations need to be performed to resolve between closely competing structures for a new compound.

1. Introduction

The prediction of the extent of solid solubility and of intermediate compound formation in alloys has interested research workers for a long time. Empirical rules were developed by Hume-Rothery et al. [1] and Darken and Gurry [2] to predict extent of solid solubility. Structure prediction has also been given great importance owing to the strong physical property–structure correlations. A wealth of experimental data is available in the literature on the crystal structures adopted by intermetallic compounds. The data has been explored on various structure maps (2-D and 3-D) and stability diagrams using elemental properties (like electronegativity, principal quantum numbers, atomic radii, etc.) by many workers like St John and Bloch [3], Zunger [4], Villars [5] and Pettifor [6]. The main aim of these maps was to predict the crystal structures of new compounds. Most of these structure maps have domains of occurrence of different shapes for each of the structure type. Rajasekharan and Girgis [7,8] had reported a linear relationship between the coordinates $\Delta\phi$ and $\Delta n_{ws}^{1/3}$ for all the compounds belonging to a particular structure type; ϕ and n_{ws} are Miedema's thermo-chemical parameters [9], and Δ denotes the difference in these parameters for the elements forming a compound. (Attempts made to construct a structure map using the absolute values $|\Delta\phi|$ and $|\Delta n_{ws}^{1/3}|$ as coordinates were unsuccessful [10]). The universality of such a linear relationship has been studied by us recently for 96 structure types with ~3000 binary compounds at different compositions [11]. The possibility of predicting concomitant and mutually exclusive structure types in binary systems was demonstrated [7,8,12]. The required data were collected from standard compilations in the literature [13–15].

It can be observed from the enormous amount of experimental information available in literature on the structures adopted by intermetallic compounds that certain structure types often occur together in binary systems, while some others are mutually exclusive. For instance, $CaCu_5$ and CsCl type compounds are often concomitant with $MgCu_2$ type compounds, whereas a $CoGa_3$ type compound or an $AsNa_3$ type compound never exists at the composition AB_3 when an $MgCu_2$ type compound occurs at AB_2 [15]. Savitskii and Gribulya [16,17] reported that the binary systems in which σ phases exist have a strong tendency to stabilize in $SiCr_3$, $MgZn_2$ and CsCl type structures at 1:3, 1:2, and 1:1 compositions respectively. They termed these structure types as 'concomitant structure types' of the σ phase. In this paper, we examine on the Rajasekharan–Girgis (*RG*) map, the behavior of all structure types that are concomitant with $MgCu_2$ type compounds in binary systems. The map is shown to be of practical value in predicting the structures of new compounds. It can be used effectively in reducing the number of candidate structures to be explored, while applying ab initio methods to the prediction of structures of intermetallic compounds. The physical origin of the ability of the $(\Delta\phi, \Delta n_{ws}^{1/3})$

* Corresponding author. Tel.: +91 40 23010241.
E-mail address: seshubai@gmail.com (V. Seshubai).

0925-8388/$ – see front matter © 2010 Elsevier B.V. All rights reserved.
doi:10.1016/j.jallcom.2010.07.219

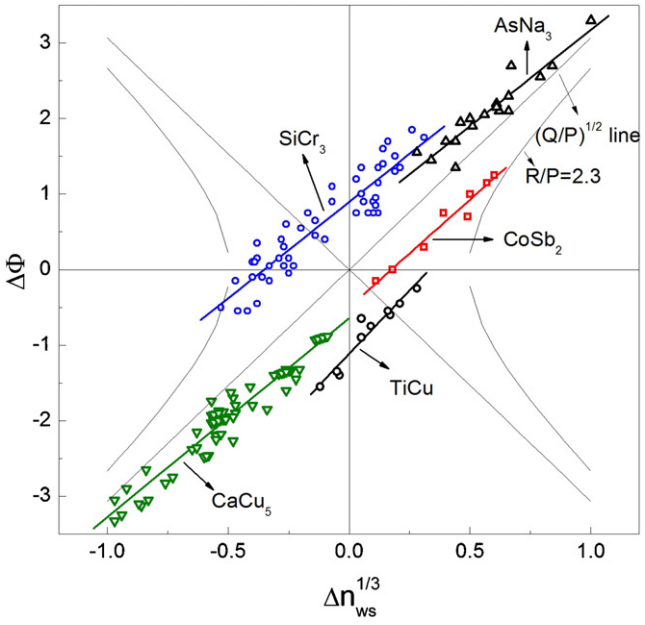

Fig. 1. *RG* lines of the structure types TiCu, $CoSb_2$, $AsNa_3$, $SiCr_3$ and $CaCu_5$ are plotted on a $(\Delta\phi, \Delta n_{ws}^{1/3})$ map. The lines are well resolved. A binary system occurring on a line corresponding to a particular structure type cannot have the other structure types considered in the figure, with the same minority element. For instance, none of the binary systems with $CaCu_5$ type compounds (at composition AB_5) will have an $AsNa_3$ type compound with A as the minority element. To find whether an $AsNa_3$ type compound can occur with B as the minority element, one has to study the overlap of the *RG* line of the $CaCu_5$ type and with the inverse *RG* line of the $AsNa_3$ type. The *RG* lines enable us to predict whether a given structure type can occur in a binary system at a particular composition.

map to predict concomitant and mutually exclusive structure types in binary systems is discussed.

We start below with a brief description of the construction of the *RG* map.

2. Construction of Rajasekharan–Girgis map

According to Miedema's macroscopic atom model [9,18–20], heat of formation of a compound (ΔH) at equiatomic composition in a binary system is equal to

$$\Delta H = \left[-(\Delta\phi)^2 + \frac{Q}{P}(\Delta n_{ws}^{1/3})^2 - \frac{R}{P}\right] \quad (1)$$

In this expression, $\Delta\phi$ and $\Delta n_{ws}^{1/3}$ are respectively the differences in work function (related to Pauling's electronegativity), and cube root of 'electron density at the boundary of Wigner–Seitz cell' (obtained from bulk modulus), of the constituent elements of the compound. P, Q and R are empirical constants which were adjusted to get the correct signs of heat of formation; $Q/P = 9.4\,\mathrm{V/(d.u.)^{1/3}}$. $R \neq 0$ only for combinations of p-metals with transition metals. The parameters ϕ and n_{ws} of the elements were adjusted by small amounts to predict, using Eq. (1), the signs of ΔH of more than 500 binary systems, with ~100% accuracy. A graphical solution of Eq. (1) says that for two transition metals, on a $(\Delta\phi, \Delta n_{ws}^{1/3})$ map, $\Delta H = 0$ on two straight lines passing through the origin with opposite slopes $\pm\sqrt{Q/P}$. (See Fig. 1). Similarly, according to Eq. (1), the alloys of transition metals with p metals (or with Be, Mg, Zn, Cd or Hg), with negative heats of formation are separated from the ones with positive heats of formation by a hyperbola given by the following equation

$$\Delta\phi = \pm\left[\frac{Q}{P}(\Delta n_{ws}^{1/3})^2 - \frac{R}{P}\right]^{1/2} \quad (2)$$

The curves located on two sides of origin in Fig. 1 correspond to $R/P = 2.3$ (the maximum value suggested by Miedema et al. [9]).

Corresponding to a binary system A–B, there can be two symmetrically opposite points on the $(\Delta\phi, \Delta n_{ws}^{1/3})$ map: $((n_{wsA}^{1/3} - n_{wsB}^{1/3}), (\phi_A - \phi_B))$ and $((n_{wsB}^{1/3} - n_{wsA}^{1/3}), (\phi_B - \phi_A))$. For a compound at the composition A_mB_n $(n > m)$, we plot $(\phi_A - \phi_B)$ versus $(n_{wsA}^{1/3} - n_{wsB}^{1/3})$. For the 1:1 composition AB, we plot $(\phi_A - \phi_B)$ versus $(n_{wsA}^{1/3} - n_{wsB}^{1/3})$, with the element A identified as the one to the left of B in the periodic table. For brevity, the straight line formed by the binary systems in which compounds of a particular structure type occur, on the $(\Delta\phi, \Delta n_{ws}^{1/3})$ map, is called as the '*RG* line', and the line that is obtained by plotting $(\phi_B - \phi_A)$ versus $(n_{wsB}^{1/3} - n_{wsA}^{1/3})$ as the '*Inverse RG* line' of the structure type [12]. We note that the composition at which a structure type occurs does not enter into deciding its coordinates on the *RG* map; thus each point on the map represents a binary system, and not a particular intermetallic compound.

3. Concomitance of structure types with $MgCu_2$ type compounds

In Fig. 1, we show on the $(\Delta\phi, \Delta n_{ws}^{1/3})$ map, the *RG* lines corresponding to the structure types TiCu, $CoSb_2$, $AsNa_3$, $SiCr_3$ and $CaCu_5$. The structure types that we have chosen are typical and have been chosen to illustrate some characteristics of the *RG* lines. The compounds occur at different compositions and there are several representatives belonging to each structure type. There are 10, 8, 20, 51 and 79 binary systems with TiCu (tP4), $CoSb_2$ (mP12), $AsNa_3$ (hP8), $SiCr_3$ (cP8) and $CaCu_5$ (hP6) type compounds respectively. In Fig. 1, we note that all the binary systems having compounds of the above crystal structures are located in regions of the map where Eq. (1) predicts a negative heat of formation. The figure shows that all the binary systems with intermetallic compounds of a particular structure type fall on a straight line with a positive slope *nearly* equal to $\sqrt{Q/P}$. We note from the figure that one can predict whether an $SiCr_3$ or $AsNa_3$ type compound is likely to occur in a particular binary system from its location on the map. From the map we can also conclude that binary systems which have compounds with $CaCu_5$ type structure at 1:5 composition, do not stabilize with $AsNa_3$ type compounds at 1:3, or $CoSb_2$ type compounds at 1:2 or TiCu type compounds at 1:1.

Laves Phases form the largest group of intermetallic compounds. They crystallize in one of the three closely related $MgCu_2$, $MgZn_2$ or $MgNi_2$ structure types. The crystal structures of Laves phases and the factors that influence their stability have been discussed very extensively in the literature [21–23]. Laves phases belong to the class of Frank–Kasper phases showing topologically close packed structures. They have the general composition AB_2 with the larger A atoms at the centre of a 16 atom (4 A and 12 B) polyhedron and the smaller B atoms at the centers of icosahedra with 12 coordination (6 A and 6 B atoms). The closest packing in $MgCu_2$ type structure is achieved with a radius ratio of 1.225 at which both A–A and B–B contacts are formed. However, many compounds with radius ratios different from the above ideal value are observed to be stabilized in this structure type [24]. The heat of formation of the $MgCu_2$ type compounds varies over a wide range [25,26]. A vast majority of the compounds belonging to these structure types are formed between rare earth elements and transition metals. Structural transitions are known to occur between several of them as a function of temperature [7,15]. The *RG* line of the $MgCu_2$ structure type with 181 binary systems is shown in Fig. 2; the binary systems in the figure form a straight line with a correlation factor of 0.95. In the figure, we have also shown the '*Inverse RG* line' of the $MgCu_2$ type. We note that the *RG* line of $MgCu_2$ structure type is located in the lower quadrants,

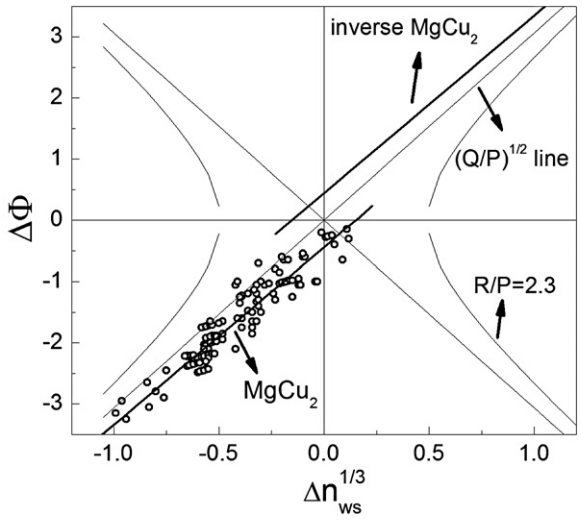

Fig. 2. 181 binary systems with $MgCu_2$ type compounds are shown by open circles on the $(\Delta\phi, \Delta n_{ws}^{1/3})$ map. They form a straight line with positive slope. The slope, intercept and regression factor of the best-fit line are given in Table 1. The inverse *RG* line of the system is also shown in the figure.

while the inverse *RG* line is located in the upper quadrants, of the map.

We have searched the phase diagrams [15] of all binary systems which contain intermetallic compounds with $MgCu_2$ type crystal structure at 1:2, for concomitant crystal structure types. Table 1 gives the 22 structure types that are concomitant with $MgCu_2$ type compounds. Only those structure types with at least 5 representative compounds are considered in our work. The total number of compounds having a particular crystal structure and the number of binary systems in which they coexist with the $MgCu_2$ type compounds are also given in the Table. Also given are the slopes and intercepts of the *RG* lines of all the structure types listed. Detailed information on the crystal structures of the compounds can be found in Pearson's book [23]. The features reflected on the *RG* map due to concomitance of the 22 structure types with the $MgCu_2$ type are illustrated below through some typical examples.

3.1. Concomitance with structure types having RG lines in the lower quadrants

In $CaCu_5$ (hP6) structure type, each A atom is surrounded by a coordination polyhedron of 18 B atoms (6 Cu atoms at a distance of 2.94 Å and 12 Cu atoms at a distance of 3.26 Å in the prototype compound) and 2 A atoms (Ca atoms at a distance of 4.09 Å in the prototype compound). Each B atom has 12 neighbors, but the arrangement is not icosahedral. The majority atom is by and large from one of the groups of Co, Ni, and Cu in the periodic table. The minority atom is either a rare earth (RE) element or an alkaline earth metal. Fig. 3 shows the *RG* line of the $CaCu_5$ structure type. The 79 binary systems with $CaCu_5$ type compounds are represented by open circles (red online) in the figure. The *RG* line of the $MgCu_2$ type structure (the best fit line only and not the points) is also shown in the figure. The 43 binary systems in which both $MgCu_2$ type (at 1:2) and $CaCu_5$ type (at 1:5) compounds occur together are marked by solid circles (black online) in the figure, and they can be observed to be located around the region of overlap of the *RG* lines of the two structure types.

64 binary systems have intermetallic compounds with FeB type structure at 1:1 composition. The prototype FeB has a primitive orthorhombic structure with 8 atoms per unit cell. The first element 'A' is a transition metal or a rare earth metal and the second element 'B' is either from Ni, Cu groups or Boron, Si, or Ge. On the $(\Delta\phi, \Delta n_{ws}^{1/3})$ map, the binary systems having FeB type compounds (open circles, red online) fall on a straight line as shown in Fig. 4. The *RG* line of $MgCu_2$ type is also shown in the figure. There are 17 binary systems of rare earth elements with Ni or Pt adopting $MgCu_2$ type structure at 1:2 composition, and FeB type structure at 1:1 composition. Those binary systems with both the structure types are shown by solid circles (black online) in the figure. It is interesting to observe that the binary systems in which both the structure types are concomitant, are located in the region where the *RG* lines overlap towards one end. It can also be observed that

Table 1
The structure types concomitant with $MgCu_2$ type compounds are listed in the second column. The total number of intermetallic compounds crystallizing in each structure type is given in the third column. The number of binary systems in which the particular structure type and $MgCu_2$ type coexist is given in column 4. Pearson's symbol and space group respectively are given in the next two columns. The slope, intercept and regression factors of the *RG* lines are given in columns 7, 8 and 9, respectively.

S. No	Prototype	No. of binary phases	No. of common phases	Pearson symbol	Space group	Details of the *RG* lines		
						Slope	Intercept	Regression factor
1	$MgCu_2$	181		cF24	$Fd\bar{3}m$	2.90	−0.44	0.95
2	CsCl	224	22	cP2	$Pm3m$	3.27	−0.53	0.93
3	CrB	105	22	oC8	$Cmcm$	2.70	−0.78	0.95
4	FeB	64	17	oP8	$Pnma$	2.58	−0.80	0.92
5	$CaCu_5$	79	43	hP6	$P6/mmm$	2.65	−0.63	0.96
6	Si_3Mn_5	145	24	hP16	$P6_3/mcm$	2.90	0.44	0.95
7	Rh_3Pu_5	15	14	tP32	$P4/ncc$	2.44	0.83	0.99
8	$CuAl_2$	51	6	tI12	$I4/mcm$	2.544.71	0.85−1.91	0.930.94
9	$SnNi_3$	62	12	hP8	$P6_3/mmc$	2.692.28	0.61−0.77	0.950.86
10	$AuCu_3$	240	20	cP4	$Pm\bar{3}m$	Multiple lines		
11	$BaAl_4$	18	7	tI10	$I4/mmm$	2.01	−0.67	0.95
12	Er_2Co_7	27	24	hR18	$R\bar{3}m$	2.72	−0.49	0.82
13	$ThMn_{12}$	32	12	tI26	$I4/mmm$	1.57	−0.65	0.70
14	Si_3W_5	39	4	tI32	$I4/mcm$	2.31	0.81	0.94
15	Ce_2Ni_7	21	17	hP36	$P6_3/mmc$	2.78	−0.47	0.61
16	Fe_3Th_7	48	29	hP20	$P6_3mc$	3.12	0.52	0.84
17	Th_2Zn_{17}	30	14	hR19	$R\bar{3}m$	2.08	−0.66	0.96
18	Th_2Ni_{17}	52	32	hP38	$P6_3/mmc$	2.42	−0.61	0.93
19	Th_6Mn_{23}	35	17	cF116	$Fm\bar{3}m$	1.91	−0.6	0.84
20	$SiCo_2$	73	16	oP12	$Pnma$	3.43	0.54	0.98
21	CFe_3	86	53	oP16	$Pnma$	1.49	1.32	0.58
22	BiF_3	29	7	cF16	$Fm\bar{3}m$	2.95	0.55	0.98
23	$NbBe_3$	46	45	hR12	$R\bar{3}m$	2.12	−0.79	0.81

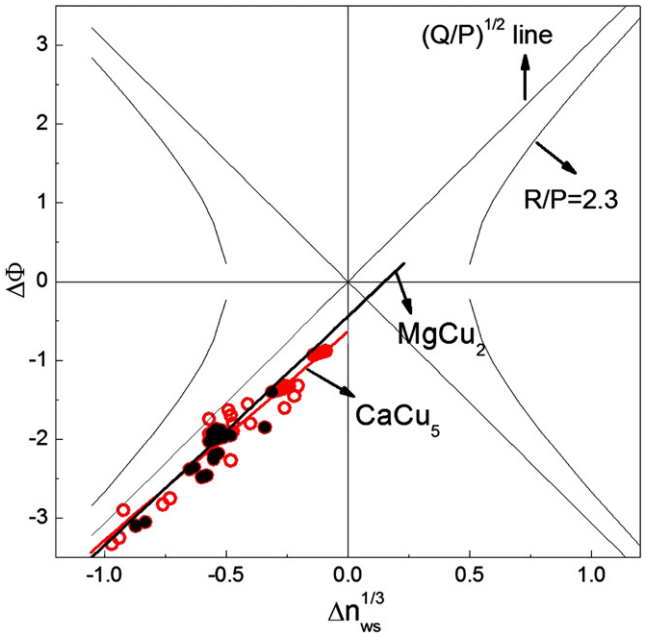

Fig. 3. The *RG* lines of $CaCu_5$ and $MgCu_2$ structure types are plotted. The binary systems with $CaCu_5$ type compounds are shown by open circles (red). The slope, intercept and regression factor of the best-fit line are given in Table 1. The *RG* line of the $MgCu_2$ structure type is represented by the best-fit line only (for clarity). The binary systems in which both the structure types coexist are denoted by solid circles, black online. The binary systems in which the structure types are concomitant are concentrated in the region of overlap of the *RG* lines. We also note the absence of such binary systems elsewhere in the ($\Delta\phi$, $\Delta n_{ws}^{1/3}$) field. (For interpretation of the references to color in this figure legend, the reader is referred to the web version of the article.)

the large number of binary systems which are located in the region where the straight lines corresponding to $MgCu_2$ and FeB structure types are well separated, have only $MgCu_2$ type or FeB type compounds, but not both the structure types.

The *RG* lines of the structure types Er_2Co_7 (hR18) and Ce_2Ni_7 (hP36) are shown in Figs. 5 and 6 respectively, along with that of the $MgCu_2$ type. Er_2Co_7 structure type has 27 compounds which are represented by open circles (red online) in Fig. 5. Most of the binary systems with this structure type (24 out of 27) have com-

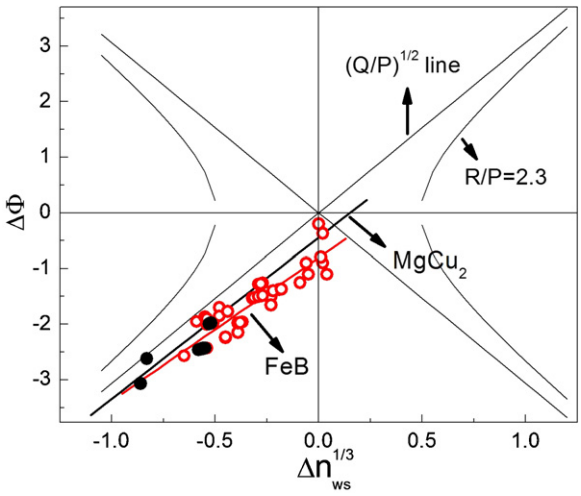

Fig. 4. The *RG* lines of FeB and $MgCu_2$ structure types are plotted. The FeB type compounds are indicated by open circles (red). The binary systems in which both the structure types coexist are denoted by solid circles. Such binary systems are concentrated in the region of overlap of the *RG* lines. (For interpretation of the references to color in this figure legend, the reader is referred to the web version of the article.)

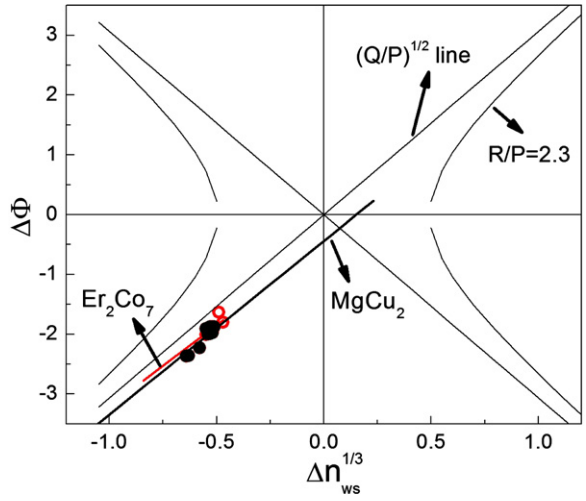

Fig. 5. The *RG* lines of Er_2Co_7 and $MgCu_2$ structure types are plotted. The *RG* line of Er_2Co_7 (27 representatives) is a short line which merges with that of $MgCu_2$ type (181 representatives). The binary systems having compounds of Er_2Co_7 type structure are marked by open circles (red) and the binary systems (24 out of 27) which have both $MgCu_2$ and Er_2Co_7 type compounds are represented by solid circles. (For interpretation of the references to color in this figure legend, the reader is referred to the web version of the article.)

pounds stabilized with $MgCu_2$ structure at 1:2 composition, and the binary systems with both Er_2Co_7 and $MgCu_2$ type compounds are shown by solid (black online) circles in the figure. Fig. 6 shows 21 binary systems in which Ce_2Ni_7 type compounds occur, by open circles (red online). The 17 binary systems in which $MgCu_2$ type is concomitant with Ce_2Ni_7 type compounds are shown in the figure by solid black circles. In most of the binary systems with the above structure types, there exist $MgCu_2$ type compounds at 1:2. This fact is reflected in the merger of the *RG* lines of the two structure types with that of the $MgCu_2$ type as seen in Figs. 5 and 6.

The unit cell of $NbBe_3$ is rhombohedral with 12 atoms per unit cell. Most of the representatives are compounds of rare earth ele-

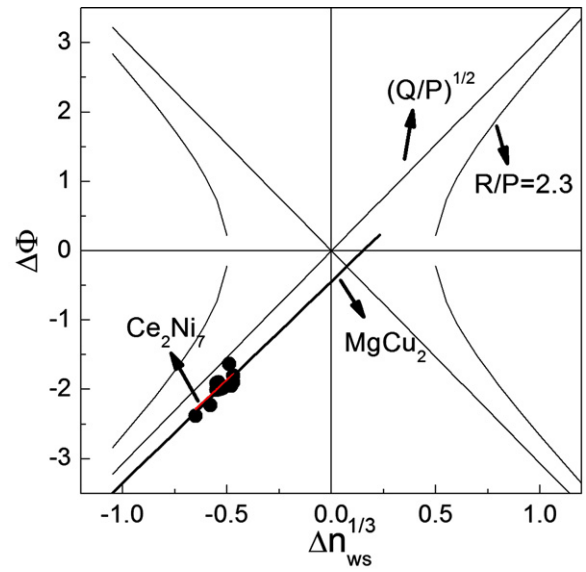

Fig. 6. The *RG* lines of Ce_2Ni_7 and $MgCu_2$ structure types are plotted. The *RG* line of Ce_2Ni_7 (21 representatives) is short and merges with the *RG* line of $MgCu_2$ type. The binary systems having compounds of Ce_2Ni_7 type structure are marked by open circles (red), and the binary systems (17 out of 21) which have both $MgCu_2$ and Ce_2Ni_7 type compounds are represented by solid circles. (For interpretation of the references to color in this figure legend, the reader is referred to the web version of the article.)

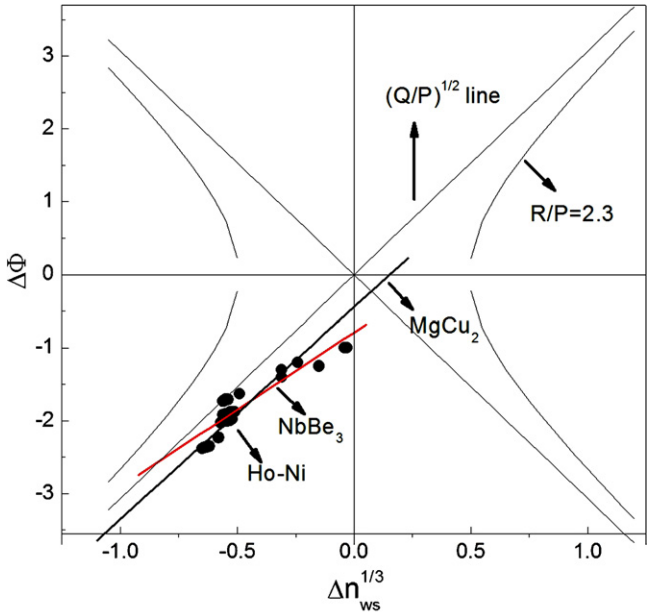

Fig. 7. The *RG* lines of $NbBe_3$ and $MgCu_2$ structure types are shown. Most of the binary systems with $NbBe_3$ type compounds have $MgCu_2$ type compounds as well (45 out of 46). The binary systems with both $MgCu_2$ type and $NbBe_3$ type compounds are marked by solid circles. In the Ho-Ni system which is marked in the figure, $HoNi_2$ is $MgCu_2$ type and $HoNi_3$ is $NbBe_3$ type.

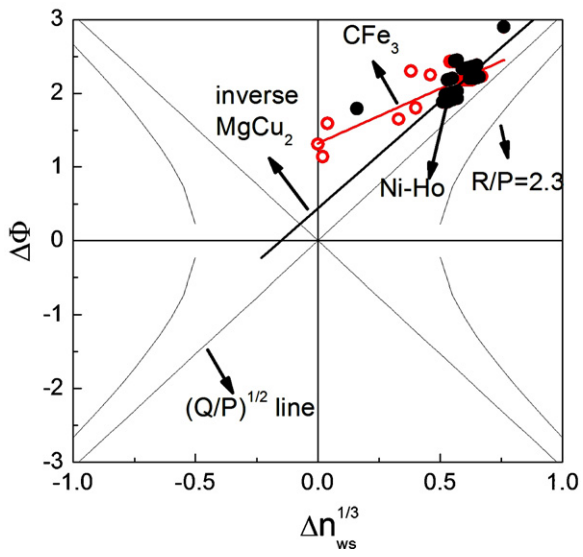

Fig. 8. The *RG* line of CFe_3 structure type (with 86 representatives), and the inverse *RG* line of $MgCu_2$ structure type are plotted together. Since many compounds of very small atoms are involved, there is more scatter on this line for CFe_3 structure type. Majority of the compounds involve rare earth elements whose Miedema parameters are nearly the same, leading to clustering. The correlation factor for the linear fit is rather poor (Table 1). The binary systems (53) with both $MgCu_2$ and CFe_3 type compounds are located close to the region of overlap of the *RG* lines. In the Ho–Ni system which is marked in the figure, $HoNi_2$ is $MgCu_2$ type and $NiHo_3$ is $NbBe_3$ type.

ments with Fe, Co or Ni. From the experimental data in the literature [15], it is observed that most (45 out of 46) of the binary systems with $NbBe_3$ type compounds at 1:3 have $MgCu_2$ type compounds at 1:2, and are located in the overlap region of the *RG* lines of both the structure types as seen in Fig. 7. All the 45 binary systems with $NbBe_3$ type compounds are seen in solid black circles.

3.2. Concomitance with structure types having RG lines in the upper quadrants

So far we have discussed those structure types whose *RG* lines occur in the same quadrant as that of the $MgCu_2$ type. We have discussed the occurrence of $CaCu_5$ type compounds at 1:5, of Er_2Co_7/Ce_2Ni_7 type compounds at 2:7, of FeB type compounds at 1:1 and of $NbBe_3$ type compounds at 1:3, when an $MgCu_2$ type compound occurs at 1:2. The concomitant compounds in the above cases occur with the minority element of the relevant $MgCu_2$ type compound as the minority element of the compounds crystallizing in the above structure types.

To study concomitance of $MgCu_2$ type compounds (occurring at AB_2) with structure types whose *RG* lines occur in the upper quadrants, we have to examine the overlap of their *RG* lines with the inverse *RG* line of $MgCu_2$ structure type. The latter is obtained by plotting $(\phi_B - \phi_A)$ versus $(n_{wsB}^{1/3} - n_{wsA}^{1/3})$ for the $MgCu_2$ type compounds. We will then be examining the concomitance of an $MgCu_2$ type compound at AB_2 in a binary system, with structure types occurring at compositions A_mB_n $(m > n)$.

CFe_3 has primitive orthorhombic structure with 16 atoms per unit cell. 87 binary systems have compounds with this structure. Most of the compounds of this structure type are combinations of transition metals with rare earths. There are 53 binary systems which have compounds with $MgCu_2$ type structure at AB_2 when CFe_3 type compounds occur at the composition A_3B. In Fig. 8, the CFe_3 type compounds are shown (open circles, red online) along with the *RG* line of that structure type. We also show the inverse *RG* line of the $MgCu_2$ structure type in the figure. The inverse *RG* line is represented by the best fit line. Those binary systems which have both the $MgCu_2$ type and CFe_3 type compounds are shown by solid black circles in the figure. As the concomitant phases involve mostly rare earths with nearly the same Miedema parameters, they are clustered together, and are located near the overlap region of the *RG* line of CFe_3 type and the inverse *RG* line of the $MgCu_2$ type.

Si_3Mn_5 structure type (hP16) has 24 out of 145 representatives concomitant with $MgCu_2$ type. The concomitance of Si_3Mn_5 type compounds with $MgCu_2$ type compounds has been discussed elsewhere [12].

3.3. Concomitance with structure types having dual RG lines

Structure types like $MoSi_2$, $CuAl_2$ and $SnNi_3$ have the representative binary systems distributed along two straight lines on the *RG* map. We discuss below the concomitance of those structure types with the $MgCu_2$ type.

$SnNi_3$ has a hexagonal structure with 8 atoms/unit cell. It is considered as a hexagonally stacked polytype of the $AuCu_3$ type structure [23]. It can be thought of as a superstructure of an hcp (hP2) substructure. Both Sn and Ni have 12 nearest neighbors. A total of 65 binary systems adopt $SnNi_3$ type structure at 1:3. The binary systems with $SnNi_3$ type compounds (shown as open circles, red online) fit into two straight lines on the $(\Delta\phi, \Delta n_{ws}^{1/3})$ map as shown in Fig. 9. The upper line comprises of p–t compounds and Al–RE compounds. The lower line has compounds of t–t, RE–t and RE–Al groups. In Fig. 10, we show a plot of the axial ratios (c/a) of $SnNi_3$ type compounds as a function of the radius ratios of the elements. We see that the compounds occur in two groups, one with a nearly constant axial ratio of 0.8, and the other with lower axial ratio values. It can also be seen that the two groups in Fig. 9 correspond to the two groups in Fig. 10. The *RG* and inverse *RG* lines of $MgCu_2$ type are also shown in the figure. They have only a small overlap with the $SnNi_3$ *RG* lines in the figure, and therefore, there are only a few binary systems in which the two structure types are concomitant. When an $MgCu_2$ type compound occurs at the composition AB_2, an $SnNi_3$ type compound can occur at the composition AB_3 when the binary system A–B is located on both the lower *RG*

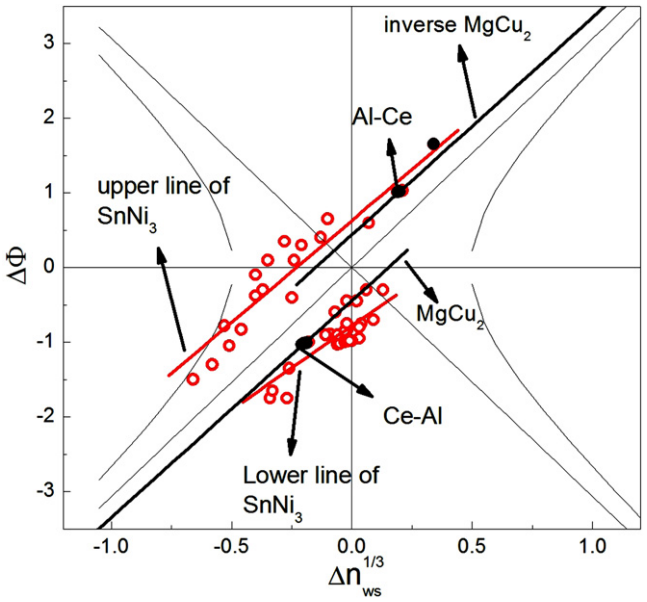

Fig. 9. Binary systems with $SnNi_3$ type compounds (open circles, red) form two lines (upper and lower) on the *RG* map. Over the most part, the two lines of $SnNi_3$ type do not overlap with the *RG* and inverse *RG* lines of $MgCu_2$ type, and there are very few binary systems with concomitant $MgCu_2$ and $SnNi_3$ type compounds. The binary systems in which the two structure types are concomitant are marked by solid circles, black online, and are located towards the region of overlap. The Ce–Al binary system marked in the figure falls on both the *RG* and inverse *RG* lines of the $MgCu_2$ type; so while $CeAl_2$ forms with $MgCu_2$ type structure, $CeAl_3$ and $AlCe_3$ form with $SnNi_3$ type structure. $AlCe_3$ corresponds to the upper *RG* line of the $SnNi_3$ type, and has an axial ratio = 0.78, as expected from Fig. 10. (For interpretation of the references to color in this figure legend, the reader is referred to the web version of the article.)

line of the $SnNi_3$ type and the *RG* line of $MgCu_2$ type. When the binary system is on the upper *RG* line of the $SnNi_3$ type and the inverse *RG* line of the $MgCu_2$ type (occurring at AB_2), an $SnNi_3$ type compound can occur at the composition A_3B. For instance in the Ce–Al binary system, while $CeAl_2$ forms with $MgCu_2$ type structure, $CeAl_3$ and $AlCe_3$ form with $SnNi_3$ type structure and fall on the corresponding lower and upper *RG* lines respectively. $AlCe_3$ has an axial ratio = 0.78, as expected from Fig. 10 for the upper line.

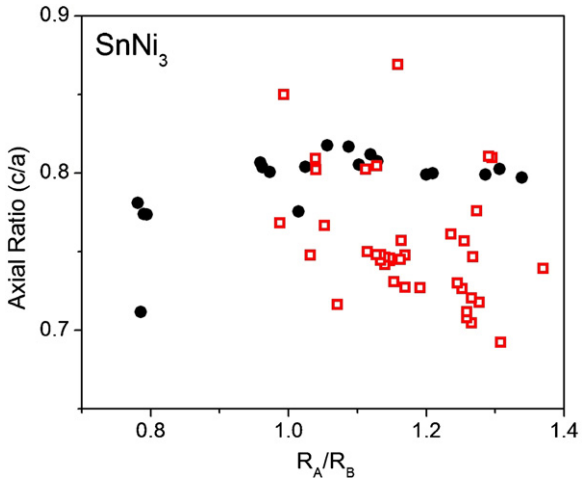

Fig. 10. c/a versus R_A/R_B for $SnNi_3$ type (hP8) compounds. Just as in the case of the $MoSi_2$ type compounds [7], the compounds of this structure type are also separated into two groups of different axial ratios, based on their location on the *RG* map (Fig. 9). The group of compounds marked by solid black circles corresponds to the upper line in Fig. 9 and has a nearly constant c/a of 0.8.

$CuAl_2$ has body centered tetragonal structure with 12 atoms per unit cell. ~50 binary systems adopt $CuAl_2$ type structure at 1:2. On the *RG* map, the binary systems with compounds of this structure type fit into two lines as shown in Fig. 11. All transition metal–p metal binary systems with $CuAl_2$ type compounds, with p-metal as the minority element, are located on the lower of the two *RG* lines. The other *RG* line has the points corresponding to t–t and t–RE compounds. A few transition metal borides, probably due to the small size of the boron atoms, deviate from both the lines and are located midway between the two lines near the origin. The deviation of binary systems from *RG* lines owing to the very small size of one of the components has been reported [7]. There are 6 binary systems which have compounds with $CuAl_2$ type structure at A_2B, with $MgCu_2$ type compounds occurring at AB_2: they are marked by solid circles in the figure. We see from the figure that the two *RG* lines of $CuAl_2$ and also the inverse *RG* line of $MgCu_2$ converge to a region in the map, and that the binary systems with concomitant structure types are located close to that overlap region.

4. Summary and discussion

In this paper we have demonstrated, by taking the concomitant structure types of the $MgCu_2$ type as examples, the efficacy of $(\Delta\phi, \Delta n_{ws}^{1/3})$ map in predicting concomitant and mutually exclusive structure types. We have studied the 22 structure types which are concomitant with $MgCu_2$ type compounds in binary phase diagrams. Several typical examples are discussed in the paper. We observe that in the case of all the structure types considered, binary systems with compounds of a particular crystal structure lie on a straight line (in a few cases, on more than one line) on the map. We observe that the *RG* lines of all structure types that are concomitant with the $MgCu_2$ type compounds overlap with the *RG*

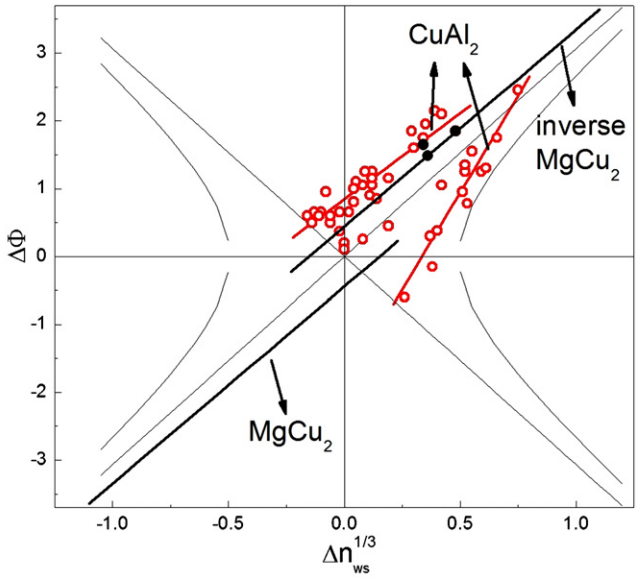

Fig. 11. The $CuAl_2$ structure type has binary systems (open circles, red) distributed along two lines (upper and lower) on the map. The points with the maximum deviation from the upper line and located towards the origin, are binary systems with small atoms like boron. The *RG* lines of $CuAl_2$ type have minimum overlap with either the *RG* line or the inverse *RG* line of the $MgCu_2$ type, thus explaining why the binary systems considered herein do not have $MgCu_2$ type compounds in spite of having elemental combinations with radius ratios close to 1.225. We see from the figure that the two *RG* lines of $CuAl_2$ and the inverse *RG* line of $MgCu_2$ converge to a region in the map. 6 binary systems with concomitant $CuAl_2$ and $MgCu_2$ compounds (marked by solid circles), are located close to the overlap region. We also note the absence of such binary systems elsewhere in the $(\Delta\phi, \Delta n_{ws}^{1/3})$ field. (For interpretation of the references to color in this figure legend, the reader is referred to the web version of the article.)

line or the inverse *RG* line of the $MgCu_2$ type in some region on the map. The concomitant compounds mostly occur in binary systems located near the point of intersection. In a binary system A–B, with an $MgCu_2$ type compound at composition AB_2, we can predict concomitant structure types at compositions A_mB_n ($m < n$) by studying the overlap of the *RG* line of the structure type with the *RG* line of the $MgCu_2$ type, and at compositions A_mB_n ($m > n$) by studying the overlap of the *RG* line of the structure type with the *inverse RG* line of the $MgCu_2$ type. Several predictions can be made regarding the crystal structures of intermetallic phases: for instance, in Ho–Ni binary system where $HoNi_2$ occurs with $MgCu_2$ type structure; the map explains the adoption of $NbBe_3$ and CFe_3 type structures by $HoNi_3$ and $NiHo_3$ respectively. In Fig. 1, we have demonstrated how the structure types which mutually exclude themselves in phase diagrams can be identified with the help of *RG* maps.

The *RG* map can be useful in the laboratory or industry when one wishes to predict the outcome of an experiment without resorting to extensive calculations. We observe from the present work that when the *RG* lines of two structure types occur close by, the binary systems with concomitant structure types tend to occur at the point of intersection of *the best-fit lines*: this seems to indicate that the parameters ϕ and n_{ws} can be further refined to make the lines thinner (by reducing the scatter) thus increasing the accuracy of the predictions. It might be recalled that Miedema et al. had refined the values of ϕ and N with the objective of accurately predicting *the signs* of the heats of formation of binary systems, and it is likely that the values of ϕ and n_{ws} can be further refined to predict stable structure types even more precisely. An alternative method of making such predictions, in principle, would be through ab initio quantum mechanical calculations. Density Functional Theory (DFT) calculations using the VASP program [27,28] have been reported to be capable of predicting the stable structure from a set of proposed structures differing in energy by only a few kcal/mol. Such calculations, for instance, would distinguish between the competing Laves phases $MgCu_2$ type, $MgZn_2$ type and $MgNi_2$ type. The *RG* lines of the Laves phase structures overlap to a degree in some regions [7] making it difficult to predict which of them would occur in the binary systems located in those regions, whereas in some other regions the lines are resolved making such predictions possible. The *RG* map minimizes the set of candidate structures on which quantum mechanical calculations need to be performed in order to identify from among competing structures, the stable structure of a new compound. We believe that digitization of the behavior of *RG* lines of all structure types would help in short listing the candidate structures for a new compound. An attempt to predict the structures of intermetallic compounds by digitizing the huge wealth of experimental data in the literature and combining the information thus obtained with quantum mechanical calculations, has been reported by Fischer et al. [29].

Miedema's parameters are isotropic in nature and the energies involved in deciding between one structure and another are quite small. Hence, apart from the tremendous practical utility of the *RG* map, there is also the interesting question of why the map predicts structures. The answer to this question has been attempted by Rajasekharan and Seshubai elsewhere [12]. According to them, each point on the *RG* map stands for the energy of the nearest neighbor atom-pair bond in a binary system and this energy remains nearly the same at all compositions in the binary system. The situation is akin to that in conventional chemistry [30] where one can define an approximate bond energy for, say, an S–H bond, and this energy would remain the same irrespective of the groups attached to the atoms constituting the bond. This fact would necessitate the *RG* lines of all structure types concomitant in a given binary system to pass through the point corresponding to that system on the map, enabling the prediction of crystal structures of intermetallic compounds as demonstrated above.

Acknowledgements

TR thanks DMRL, Hyderabad for permission to publish this article. VLK is grateful to Aurora's Technological and Research Institute, Hyderabad for sanction of leave and permission to pursue Doctoral work.

References

[1] W. Hume-Rothery, R.E. Smallman, C.W. Haworth, Structure of Metals and Alloys, 5th ed., Institute of Metals, London, 1969.
[2] L.S. Darken, R.W. Gurry, Physical Chemistry of Metals, McGraw-Hill, New York, 1953.
[3] J. St John, A.N. Bloch, Phys. Rev. Lett. 33 (1974) 1095.
[4] A. Zunger, Phys. Rev. Lett. 44 (1980) 582.
[5] P. Villars, J. Less Common Met. 92 (1983) 215.
[6] D.G. Pettifor, in: R.W. Cahn, P. Haasen (Eds.), Physical Metallurgy, North-Holland, Amsterdam, 1983.
[7] T. Rajasekharan, K. Girgis, Phys. Rev. B 27 (1983) 910.
[8] T. Rajasekharan, K. Girgis, J. Less Common Met. 92 (1983) 163.
[9] A.R. Miedema, P.F. de Chatel, F.R. de Boer, Physica B 100 (1980) 1.
[10] Zunger A, in: M. O'Keefe, A. Navrotsky (Eds.), Structure and Bonding in Crystals, vol. 1, New York Academic, 1981, p. P129.
[11] V.L. Kameswari, Regularities in the structures adopted by intermetallic compounds in binary systems, A PhD Thesis submitted to School of Physics, University of Hyderabad, Hyderabad, India, June 2008.
[12] T. Rajasekharan, V. Seshubai, Intermetallics 18 (2010) 666.
[13] W.B. Pearson, A Handbook of Lattice Spacings and Structures of Metals and Alloys, Pergamon Press, Oxford, 1967.
[14] P. Villars, L.D. Calvert, Pearson's Handbook of Crystallographic Data for Intermetallic Phases, American Society for Metals, Metals Park, OH 44073, 1985.
[15] Binary Alloy Phase Diagrams, 2nd edition plus updates on CD, T.B. Massalski (Ed. In Chief), ASM International, Materials Park, OH 44073, 1990.
[16] E.M. Savitskii, V.B. Gribulya, Dokl. Acad. Nauk. SSSR 223 (1975) 1383.
[17] E.M. Savitskii, V.B. Gribulya, Sov. Phys. Dokl. 223 (1975) 414.
[18] A.R. Miedema, R. Boom, F.R. de Boer, J. Less Common Met. 41 (1975) 283.
[19] R. Boom, F.R. de Boer, A.R. Miedema, J. Less Common Met. 45 (1976) 237.
[20] A.R. Miedema, Physica B 182 (1992) 1.
[21] M.V. Nevitt, in: A. Paul, Beck (Eds.), Electronic structure and Alloy Chemistry of the Transition Elements, Interscience Publishers a division of John Wiley & Sons, New York, 1962.
[22] C.S. Barrett, T.B. Massalski, Structure of Metals, McGraw-Hill, New York, 1968.
[23] W.B. Pearson, The crystal chemistry and physics of metals and alloys, Wiley-Interscience, New York, 1972.
[24] F. Stein, M. Palm, G. Sauthoff, Intermetallics 12 (2004) 713.
[25] J.H. Zhu, C.T. Liu, L.M. Pike, P.K. Liaw, Intermetallics 10 (2002) 579.
[26] J.H. Zhu, C.T. Liu, L.M. Pike, P.K. Liaw, Metall. Mater. Trans. A 30 (1999) 1449.
[27] G. Kresse, J. Furthmuller, Phys. Rev. B 54 (1996) 11169.
[28] G. Kresse, J. Furthmuller, Comput. Mater. Sci. 6 (1996) 15.
[29] C.C. Fischer, K.J. Tibbetts, D. Morgan, G. Ceder, Nat. Mater. 5 (2006) 641.
[30] Jolly WL, Modern Inorganic Chemistry, 2nd ed., McGraw Hill, Inc., N.Y., 1991, p. 61.